Supplementary information

I. Simplified growth factor model

In this section, we describe the details of the simple growth factor model used to generate synthetic data and the procedure to fit data to infer the parameter distribution using the maximum entropy approach as well as the discretized Bayesian approach of Hasenauer et al. (*1*).

The model comprised three species: the extracellular ligand L, inactive ligand-free cell surface receptors R, and active ligand-bound cell surface receptors P. The dynamics of the three variables was dictated by five parameters: the rate of ligand binding to inactive receptors k_1, the rate of ligand unbinding from active receptors k_{-1}, the rate of removal of inactive receptors k_{deg}, the rate of removal of active receptors k^*_{deg}, and the steady state cell surface receptor level in the absence of the ligand R_T. See SI Figure 1 for an illustration.

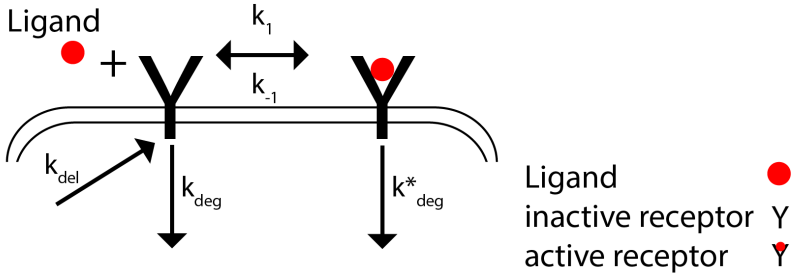

SI Figure 1: A schematic describing the dynamics of the simplified growth factor model. Growth factor molecules (red circles) bind to empty inactive receptors on the cell surface and activate them. The inactive receptors are delivered on the cell surface at a rate k_{del} and the inactive and the active receptors are removed from the cell surface at a rate k_{deg} and k^*_{deg} respectively.

In the model, the dynamics of the species are governed by the following two equations:

$$\frac{d[R]}{dt} = k_{del} - k_1[L][R] + k_{-1}[P] - k_{deg}[R] \quad \text{(S1)}$$

$$\frac{d[P]}{dt} = k_1[L][R] - k_{-1}[P] - k^*_{deg}[P] \quad \text{(S2)}$$

We simulated the model to generate synthetic data as follows. We fixed three parameters $k_1 = \frac{1}{min \cdot \frac{ng}{ml}}$, $k_{-1} = 10/min$, and $k_{deg} = 0.01/min$. We generated single cell distribution by varying the rate k^*_{deg} and the steady state abundance of cell surface receptors R_T. The rate of delivery of receptors to the cell surface was set equal to $k_{del} = R_T k_{deg}$. The rates k^*_{deg} were sampled from a gamma distribution as follows. We first generated a gamma distributed random variables *X* with a mean of 0.2/minute and a standard deviation of ~0.16/minute. We defined $k^*_{deg} = 0.55 - X$ and only included k^*_{deg} values that were between 0.1/minute and 0.5/minute. The steady state receptor abundances R_T were sampled from a gamma distribution with a mean of 4x10^5 receptors per cell and a standard deviation of ~1.27x10^5 receptors per cell. We only included receptor abundances between 2.5x10^5 and 8x10^5 receptors per cell.

We sampled 2x10^5 randomly distributed rate constants according to the abovementioned distributions and simulated signaling network output: the abundance [*P*] of active receptors at two different ligand concentrations L = 2 ng/ml and L = 10 ng/ml and two time points, t = 10 minutes, and the steady state. The four distributions were binned in 52 (L=2, t=10), 82 (L=2, steady state), 102 (L=10, t=10), and 102 (L=10, steady state) bins respectively. These constituted the "experimental" bin fractions $\bar{\phi}$.

We used the ground truth bin fractions to infer the parameter distribution using MERIDIAN and a previously developed discretized Bayesian (DB) approach by Hasenauer et al. (*1*). In MERIDIAN, the bin fractions corresponded to 338 Lagrange multipliers. The Lagrange multipliers were determined using the procedure described in section IV below. Once the Lagrange multipliers were numerically optimized, multiple parameters k^*_{deg} and R_T were sampled for further comparison.

In the DB approach, we approximated the parameter distribution as a linear combination

$$P\left(k^*_{deg}, R_T\right) = \sum \gamma_k \Phi_k\left(k^*_{deg}, R_T\right) \quad \text{(S3)}$$

where $\Phi_k\left(k^*_{deg}, R_T\right)$ are bivariate Gaussian distributions situated on an equally spaced *N*x*N* Cartesian grid and γ_k are the corresponding weights. Similar to Hasenauer et al. (*1*) we opted for *N* = 10. We fixed the covariance matrix (*1*): $\Sigma = diag\left(\sigma^2_{k^*_{deg}}, \sigma^2_{R_T}\right)$ where $\sigma_{k^*_{deg}} = 0.5\times\frac{0.4}{N}$ and $\sigma_{R_T} = 0.5\times\frac{6.5\times10^5}{N}$. For every value of *k*, we sampled $N_{sim} = 10^3$ parameter points from the bivariate Gaussian distribution $\Phi_k\left(k^*_{deg}, R_T\right)$ and estimated the predicted bin fractions $\bar{\psi}_k$ corresponding to each $\Phi_k\left(k^*_{deg}, R_T\right)$ function. The overall predicted bin fractions for the i^{th} bin is then expressed as the linear combination

$$\psi_i = \sum \gamma_k \psi_{ki}\,. \tag{S4}$$

The weights $1 > \gamma_k > 0$ were determined by minimizing the L_2 error between predicted bin fractions ψ_i and the "experimental" bin fractions $\bar{\phi}$. In the original DB approach, the weight coefficients γ_k are determined by maximizing the likelihood of observing the data. L_2 error minimization is an equivalent approach.

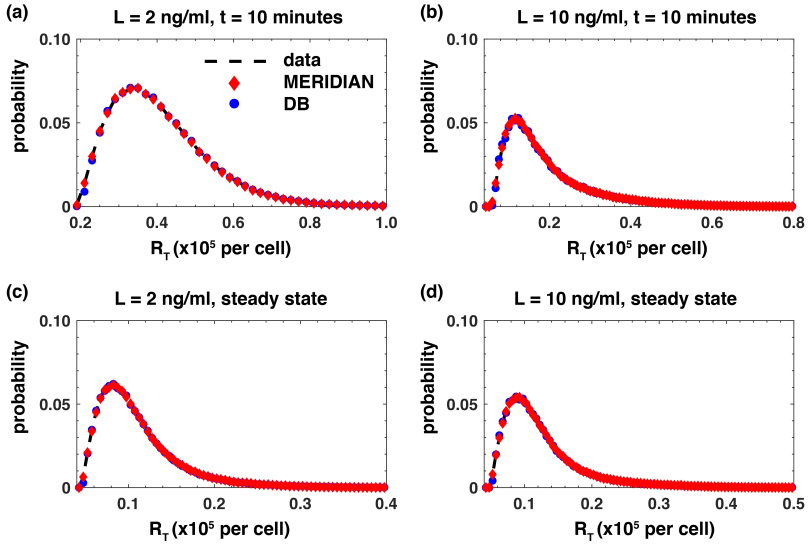

SI Figure 2: We show the synthetically generated distribution of activated receptor levels (dashed black lines) and the corresponding fits using MERIDIAN (red diamonds) and the DB approach (blue circles).

In SI Figure 2 we show the comparison between the synthetic data (dashed black lines), the MERIDIAN fits (red diamonds), and DB fits (blue circles). The comparisons between the inferred parameter distributions are plotted in Figure 3 in the main text.

Finally, we note that as the parameter space gets larger, pre-computing the predicted fractions ψ_{ki} becomes computationally unfeasible. For example, for a signaling network described by *D* parameters, the number of times the differential equations describing the signaling network need to be solved to estimate all predicted fractions ψ_{ki} is equal to $E \times N_{sim} \times N^D$ where *E* is the number of experimental conditions used to fit the distribution (*E*=4 here). For a moderately sized signaling network described *D* = 10 parameters, the number of required computations is equal to $4 \times 10^3 \times 10^{10} \sim 10^{13}$. Consequently, the DB approach is computationally unfeasible for realistic signaling networks with more than 10 parameters.

II. The EGF/EGFR signaling model

In this section, we describe in detail the dynamical model used to simulate levels of phosphorylated Akt as well as cell surface EGFRs after stimulation of cells with EGF.

The model of EGF/EGFR dependent phosphorylation of Akt was based on the previous work of Chen *et al*. (*2*). We retained the branch of the Chen *et al*. model that leads to phosphorylation of Akt subsequent to EGF stimulation. The model had 18 species and 23 parameters. The description of the species is given in SI Table 1. The description of the parameters is given in SI Table 2. A system of ordinary differential equations describing dynamics of concentrations of species participating in signaling is given in SI Equations 1. These model described EGF binding to EGFRs, subsequent receptors dimerization, phosphorylation, dephosphorylation, receptors internalization, degradation and delivery to cell surface and activation of Akt. We denote by active receptors phosphorylated receptors and by inactive receptors all other receptor states. We simplified the phosphorylation of pAkt through pEGFR; we implemented direct

interaction between pEGFR and Akt leading to phosphorylation of Akt. In agreement with the literature only cell surface-localized phosphorylated receptors were allowed to activate Akt(*3*).

Species name	Species symbol
Free EGF	u
Free EGFR monomer	R
Internalized free EGFR monomer	R_i
EGF bound EGFR monomer	B
Internalized EGF bound EGFR monomer	B_i
1 EGF bound EGFR dimer	D_1
Internalized 1 EGF bound EGFR dimer	D_{1i}
2 EGF bound EGFR dimer	D_2
Internalized 2 EGF bound EGFR dimer	D_{2i}
Phosphorylated 1 EGF bound EGFR dimer	P_1
Internalized phosphorylated 1 EGF bound EGFR dimer	P_{1i}
Phosphorylated 2 EGF bound EGFR dimer	P_2
Internalized phosphorylated 2 EGF bound EGFR dimer	P_{2i}
Unphosphorylated Akt	Akt
Phosphorylated Akt	$pAkt$
P1 bound to Akt	P_{1Akt}
P2 bound to Akt	P_{2Akt}

SI Table 1: Table of description of species and the corresponding symbols used in the differential equations.

Rate description (and references)	Variable	lower bound (log 10)	upper bound (log 10)	Units
EGF binding to EGFR(*4*)	k_1	-2.3	-1.3	$(ng/ml)^{-1}$ sec^{-1}
EGF unbinding from EGFR(*2*)	k_{-1}	-1.0	0.0	sec^{-1}
EGF-EGFR and EGFR dimerization(*2*)	k_2	-4.2	-3.2	a. u.
EGF-EGFR-EGFR undimerization(*2*)	k_{-2}	-2.0	-1.0	sec^{-1}
EGFR dimer phosphorylation(*2*)	k_{ap}	-0.5	0.5	a. u.
p-EGFR dephosphorylation(*5*)	k_{dp}	-1.5	-0.5	sec^{-1}
degradation of active EGFRs(*6*)	k^*_{deg}	-3.0	-2.0	sec^{-1}
degradation of inactive EGFRs(*7*)	k_{deg}	-4.1	-3.1	sec^{-1}
EGFR delivery to the membrane	k_{syn}	-2.2	-1.2	a. u.
Internalization of inactive EGFRs(*8*)	k_i	-4.0	-3.0	sec^{-1}
Recycling rate of inactive EGFR(*9*)	k_{rec}	-4.0	-3.0	sec^{-1}
Internalization of active EGFRs(*8*)	k^*_i	-3.0	-2.0	sec^{-1}
Recycling rate of active EGFRs(*9*)	k^*_{rec}	-4.9	-3.9	sec^{-1}
effective rate of p-EGFR binding to Akt	k_{bind}	-3.5	-2.0	a. u.
effective rate of p-EGFR unbinding from pEGFR-Akt	k_{db}	-0.7	0.8	sec^{-1}
Rate of pAkt dephosphorylation	k_p	-1.75	-0.25	sec^{-1}
Rate of Akt phosphorylation	k_a	-0.5	1.0	sec^{-1}
Total Akt abundance	Akt	0.82	4.11	a. u.
Background fluorescence in pAkt	b_0	0	0.23	a.u.
Background fluorescence in sEGFR	s_0	0	0.22	a.u.

SI Table 2: Description of model parameters. All bounds except for abundances and background fluorescence levels are in log10 units.

$$\frac{dR}{dt} = k_{syn} - k_1 uR + k_{-1}B - k_i R + k_{rec}R_i - k_2 RB + k_{-2}D_1 \tag{A1}$$
$$\frac{dR_i}{dt} = k_i R - k_{rec}R_i - k_{deg}R_i \tag{A2}$$
$$\frac{dB}{dt} = k_1 uR - k_{-1}B - k_2 RB + k_{-2}D_1 - 2k_2 B^2 + 2k_{-2}D_2 - k_i B + k_{rec}B_i \tag{A3}$$
$$\frac{dB_i}{dt} = k_i B - k_{rec}B_i - k_{deg}B_i \tag{A4}$$
$$\frac{dD_1}{dt} = k_2 RB - k_{-2}D_1 - k_{ap}D_1 + k_{dp}P_1 - k_1 uD_1 + k_{-1}D_2 - k_i D_1 + k_{rec}D_{1i} \tag{A5}$$
$$\frac{dD_{1i}}{dt} = k_i D_1 - k_{rec}D_{1i} - k_{deg}D_{1i} + k_{dp}P_{1i} - k_{ap}D_{1i} \tag{A6}$$
$$\frac{dD_2}{dt} = k_2 B^2 - k_{-2}D_2 - k_i D_2 + k_{rec}D_{2i} - k_{ap}D_2 + k_{dp}P_2 + k_1 uD_1 - k_{-1}D_2 \tag{A7}$$
$$\frac{dD_{2i}}{dt} = k_i D_2 - k_{rec}D_{2i} - k_{deg}D_{2i} + k_{dp}P2i - k_{ap}D_{2i} \tag{A8}$$
$$\frac{dP_1}{dt} = k_{ap}D_1 - k_{dp}P_1 - k_1 uP_1 + k_{-1}P_2 - k_i^* P_1 + k_{rec}^* P_{1i} - k_{bind}P_1 Akt + k_{db}P_{1Akt} + k_a P_{1Akt} \tag{A9}$$
$$\frac{dP_{1i}}{dt} = k_i^* P_1 - k_{rec}^* P_{1i} - k_{deg}^* P_{1i} - k_{dp}P_{1i} + k_{ap}D_{1i} \tag{A10}$$
$$\frac{dP_2}{dt} = k_{ap}D_2 - k_{dp}P_2 + k_1 uP_1 - k_{-1}P_2 - k_i^* P_2 + k_{rec}^* P_{2i} - k_{bind}P_2 Akt + k_{db}P_{2Akt} + k_a P_{2Akt} \tag{A11}$$
$$\frac{dP_{2i}}{dt} = k_i^* P_2 - k_{rec}^* P_{2i} - k_{deg}^* P_{2i} - k_{dp}P_{2i} + k_{ap}D_{2i} \tag{A12}$$
$$\frac{dP_{1Akt}}{dt} = k_{bind}P_1 Akt - k_{db}P_{1Akt} - k_a P_{1Akt} \tag{A13}$$
$$\frac{dP_{2Akt}}{dt} = k_{bind}P_2 Akt - k_{db}P_{2Akt} - k_a P_{2Akt} \tag{A14}$$
$$\frac{dpAkt}{dt} = k_a \left(P_{1Akt} + P_{2Akt}\right) - k_p pAkt \tag{A15}$$
$$\frac{dAkt}{dt} = -k_{bind}Akt \left(P_1 + P_2\right) + k_{db} \left(P_{1Akt} + P_{2Akt}\right) + k_p pAkt \tag{A16}$$

SI Equations 1 Differential equations that describe time evolution of species in the model

III. Experimental procedures

In this work, we used distributions of cell-to-cell variability in phosphorylated Akt levels as well as cell surface EGFR levels. We used the experimental data on pAkt levels previously measured in Lyashenko *et al.*(*10*) We measured cell-to-cell variability in sEGFR levels in this work. Briefly, we describe the experimental methods here.

MCF 10A cells were obtained from the ATCC. The cells were grown according to ATCC recommendations. We confirmed the cell identity by short tandem repeat (STR) profiling at the Dana-Farber Cancer Institute. We tested the cells with MycoAlert PKUS mycoplasma detection kit (Lonza) and ensured that

they were free of mycoplasma infection. For the experiments, we coated 96 well plates (Thermo Fisher Scientific) with type I collagen from rat tail (Sigma-Aldrich) by incubating plates with 65 microliter of 4mg/ml collagen I solution in PBS for two hours at room temperature. We washed the plates twice with PBS using EL406 Microplate Washer Dispenser (BioTek) and sterilized them under UV light for 20 minutes prior to use. Cells were harvested during logarithmic growth. We dispensed 2500 cells per well into collagen-coated 96 well plates using a EL406 Microplate Washer Dispenser. We grew the cells in 200 microliter of complete medium for 24 hours. The cells were serum-starved twice in starvation media (DMEM/F12 supplemented with 1% penicillin-streptomycin and 0.1% bovine serum albumin). Next, we incubated the cells in 200 microliter of starvation media for 19 hours and again for one more hour. This time point constituted t=0 for all experiments.

We created the EGF treatment solutions by dispensing the appropriate amounts of epidermal growth factor (EGF, Peprotech) into starvation media using a D300 Digital Dispenser (Hewlett-Packard). To fit the parameter distributions, we used EGF concentrations of 0.1, 0.31, 3.16, 10, and 100 ng/ml for Akt phosphorylation measurements and EGF concentrations of 0, 1, and 100 ng/ml for surface EGFR measurements. At t=0 cells were stimulated with 100 microliter of 3x solution and incubated for indicated times (5, 15, 30, and 45 minutes for pAkt and 180 minutes for sEGFR). To test the model predictions, we collected pAkt distributions at 90 and 180 minutes after stimulation with 0.01, 0.031, 0.1, 0.31, 1, 3.16, 10, 31.6, and 100 ng/ml EGF. We also measured sEGFR distributions at 180 minutes after stimulation with 0.0078, 0.0156, 0.0312, 0.0625, 0.125, 0.25, 0.5, 1, and 100 ng/ml of EGF. All incubations were terminated by adding 100 µl of 12% formaldehyde solution (Sigma) in phosphate buffered saline (PBS) and fixing the cells for 30 min at room temperature.

We performed all subsequent washes and treatments with the EL406 Microplate Washer Dispenser. We washed the cells twice in PBS and permeabilized them with 0.3% Triton X-100 (Sigma-Aldrich) in PBS for 30 min at room temperature. Cells were washed once again in PBS, and blocked in 40

microliter of Odyssey blocking buffer (LI-COR Biotechnology) for 60 min at room temperature. Cells were incubated with 30 microliter of anti-phospho-Akt (Cell Signaling Technologies, #4060, 1:400) or anti-EGFR (Thermo Fisher Scientific, MA5-13319, 1:100) over night at 4°C. We then washed the cells once in PBS and three time in PBS with 0.1% Tween 20 (Sigma-Aldrich; PBS-T for 5 min each and incubated with 30 microliter of a 1:1000 dilution of Alexa Fluor 647 conjugated goat anti-rabbit or goat anti-mouse secondary antibody in Odyssey blocking buffer for 60 min at room temperature. Next we washed the cells two times in PBS-T, once with PBS, and stained for 30 min at room temperature with whole cell stain green (Thermo Fisher Scientific) and Hoechst (Thermo Fisher Scientific). Finally, cells were washed three times in PBS, covered in 200 microliter of PBS, and sealed for microscopy. We imaged cells with an Operetta high content imaging system (Perkin Elmer) and analyzed the resulting scans using the Columbus image data storage and analysis system (Perkin Elmer). We performed the experiments in biological triplicates for surface EGFR and quadruplets for pAkt. In order to directly compare the different repeats, we normalized sEGFR measurements in individual repeats by the population average sEGFR levels at 0 ng/ml EGF. We normalized the pAkt levels in individual repeats by the population average pAkt levels when cells were exposed to 100 ng/ml of EGF for 5 minutes.

IV. Numerical determination of the parameter distribution

IV.1 Binning experimental data

To infer the joint distribution over model parameters, we used 24 measured distributions of cell-to-cell variability (20 pAkt distributions, 1 pAkt background fluorescence distribution and 3 sEGFR distributions, see below). For each measured distribution we used 11 bins. The locations and widths of the bins were chosen to fully cover the observed abundance range while also ensuring reliable estimates of the bin fractions ϕ_{ij}. See supplementary data for bin locations and experimentally estimated bin fractions.

We detected a small but significant pAkt signal in the absence of EGF stimulation. This background fluorescence signal likely originated from off target binding of pAkt-detecting antibodies. We assumed that the fluorescent readouts of pAkt/sEGFR levels in individual cells were equal to the sum of EGF dependent pAkt/sEGFR levels as computed using the signaling network model and the cell-dependent, but time-independent background fluorescence signal. In case of pAkt levels, the distribution of the background fluorescence was fitted to the experimentally measured distribution of the background fluorescence (pAkt readout without EGF stimulation). Unlike pAkt levels that respond to stimulation with EGF, cells maintain a high number of EGF receptors on the cell surface in the absence of EGF. As a result, we did not have experimental access to 'background fluorescence' distribution for sEGFR-detecting antibodies. We determined the range of background sEGFR fluorescence levels as follows. At the highest saturating dose of EGF (100 ng/ml) majority of the cell surface EGFRs are likely to be removed from the cell surface and degraded. At this dose, the maximum observed surface EGFR levels in the data was equal to 0.4 a. u. We assumed that the sEGFR background fluorescence can account for half of the measured fluorescence. We did not fit the distribution of background sEGFR levels to a specific distribution.

IV.2 Numerical search for the Lagrange multipliers

The numerical search for Lagrange multipliers that are associated with bin fractions is a convex optimization problem. We resorted to a straightforward and stable algorithm proposed in (*11*). The algorithm proceeded as follows. We started the calculations with an initial guess for the Lagrange multipliers as $\lambda_{0,ij} \propto -\log \phi_{ij}$ for each of the 11 bins of the 24 fitted distributions. In the n^{th} iteration, using the Lagrange multipliers $\bar{\lambda}_n$, we estimated the predicted bin fractions $\bar{\psi}_n$ using Markov chain Monte Carlo (MCMC) sampling.

MCMC sampling in each iteration was performed as follows. We propagated 100 parallel Markov Chain Monte Carlo (MCMC) chains starting at random points in the parameter space. Individual MCMC chains in the parameter

space were run as follows. In the MCMC, on an average 5 parameters were changed in a single Monte Carlo step. The parameters were constrained to be within the upper and lower limits determined individually for each parameter based on available literature estimates (see SI Table 2). Each chain was run for 25000 MCMC steps. At each step, we solved the system of differential equations given in SI equations 1 numerically with the proposed parameter assignment. We evaluated the pAkt and sEGFR levels and accepted the proposed parameters using the Metropolis criterion applied to equation (4) in the main text. Parameter points that predicted pAkt and sEGFR levels outside of the ranges observed in experimental data were rejected (see supplementary data for ranges). We discarded the first 3000 steps as equilibration and saved parameter values every 50th iteration. At the end of the calculation, parameter samples from all MCMC chains were combined together. We also imposed a few realistic constraints on pAkt and sEGFR time courses predicted by the model. All parameter sets that did not satisfy these constraints were discarded. The constraints were as follows. (1) Given that EGF ligand induces receptor endocytosis, we required that the surface EGFR levels at 180 minutes of sustained stimulation with 100 ng/ml EGF to be lower than the steady state surface EGFR levels in the absence of EGF stimulation. (2) Similarly we required that pAkt levels at 45 minutes were lower than pAkt levels at 5 minutes across all EGF stimulations used to constrain pAkt distributions (0.1, 0.31, 3.16, 10, and 100 ng/ml).

Using the sampled parameters, we estimated the bin fractions $\bar{\psi}_n$ as well as the elements of the relative error vector $\bar{\Delta}_{n,i} = (\psi_{n,i} - \phi_i)/\phi_i$ in the n^{th} iteration. For the n+1st iteration, we proposed new multipliers $\bar{\lambda}_{n+1} = \bar{\lambda}_n + \alpha_n \bar{\Delta}_n$. The multiplication constant α_n was chosen as follows. First, the approximate estimate of the predicted bin fractions for a given value of α_n was obtained using the Taylor series expansion

$$\psi_{n+1,i}(\alpha_n) \approx \psi_{n,i} + \sum_j \left(\lambda_{n+1,j} - \lambda_{n,j}\right) \frac{d\psi_{n,i}}{d\lambda_j} \Big| \lambda_j = \lambda_{n,j} \qquad \text{(S5)}$$

where

$$\frac{d\psi_{n,i}}{d\lambda_j} = -\left(\left\langle I_i I_j \right\rangle_{\bar{\lambda}_n} - \psi_{n,i}\psi_{n,j}\right) \quad \text{(S6)}$$

is the negative of the covariance between bin fractions when the Lagrange multipliers are fixed at $\bar{\lambda} = \bar{\lambda}_n$. We chose a_n in the interval [0.05, A_n] so as to minimize the relative error $e_n = \sum_i \left|\Delta_{n,i}\right|$. The maximum allowed value of a_n was decreased in schedules. We ran the calculation in 3 schedules. In each schedule, we continued with the Lagrange multipliers obtained at the last iteration of the previous schedule. We chose A_n = 0.3 for iteration number 1 to 15, A_n = 0.2 for iteration number 16 to 25, and A_n = 0.1 for iteration number 25 to 30.

The median error per bin was ~12% for the final value of the Lagrange multipliers. 1000 MC steps took 2-3 minutes. The search for the Lagrange multipliers was completed within 2 days. At the end of the calculation, the numerically inferred distribution over parameters captured with high accuracy the individual bin fractions of the distributions that were used to constrain it (Pearson's r^2 = 0.84, $p < 10^{-10}$, median relative error = 12%). Notably, as seen in SI Figure 3, the predicted bin fractions from two independent calculations to determine the Lagrange multipliers were highly correlated with each other (Pearson's r^2 = 0.98, $p < 10^{-10}$) indicating that the calculations converged to the same parameter distribution.

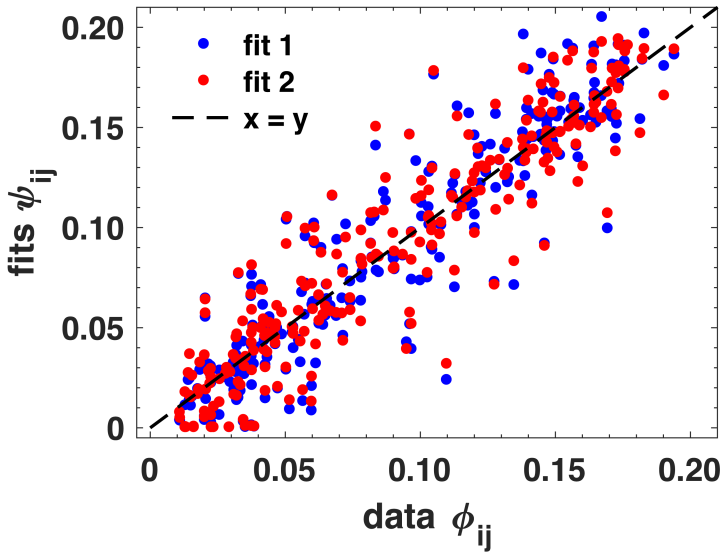

SI Figure 3: The correlation between experimentally estimated bin fractions (x axis) and predicted bin fractions (y axis) for two independent searches for the Lagrange multipliers (red and blue dots).

References

1. J. Hasenauer *et al.*, Identification of models of heterogeneous cell populations from population snapshot data. *BMC Bioinformatics* **12**, 125 (2011).
2. W. W. Chen *et al.*, Input-output behavior of ErbB signaling pathways as revealed by a mass action model trained against dynamic data. *Mol Syst Biol* **5**, 239 (2009).
3. K. M. Nicholson, N. G. Anderson, The protein kinase B/Akt signalling pathway in human malignancy. *Cell Signal* **14**, 381-395 (2002).
4. B. Schoeberl, C. Eichler-Jonsson, E. D. Gilles, G. Muller, Computational modeling of the dynamics of the MAP kinase cascade activated by surface and internalized EGF receptors. *Nat Biotechnol* **20**, 370-375 (2002).
5. L. B. Kleiman, T. Maiwald, H. Conzelmann, D. A. Lauffenburger, P. K. Sorger, Rapid phospho-turnover by receptor tyrosine kinases impacts downstream signaling and drug binding. *Mol Cell* **43**, 723-737 (2011).
6. B. S. Hendriks, H. S. Wiley, D. Lauffenburger, HER2-mediated effects on EGFR endosomal sorting: analysis of biophysical mechanisms. *Biophys J* **85**, 2732-2745 (2003).
7. H. Shankaran *et al.*, Integrated experimental and model-based analysis reveals the spatial aspects of EGFR activation dynamics. *Mol Biosyst* **8**, 2868-2882 (2012).
8. H. S. Wiley *et al.*, The role of tyrosine kinase activity in endocytosis, compartmentation, and down-regulation of the epidermal growth factor receptor. *J Biol Chem* **266**, 11083-11094 (1991).
9. J. J. Herbst, L. K. Opresko, B. J. Walsh, D. A. Lauffenburger, H. S. Wiley, Regulation of postendocytic trafficking of the epidermal growth factor

receptor through endosomal retention. *J Biol Chem* **269**, 12865-12873 (1994).
10. E. N. Lyashenko, M. Dixit, P. D. Lim, S. K. Sorger, P. Vitkup D. , Receptor-based mechanism of relative sensing in mammalian signaling networks. (2017).
11. G. Tkacik, E. Schneidman, M. J. Berry, 2nd., W. Bialek, Ising models for networks of real neurons. *arXiv* **q-bio/0611072**, (2006).